# VIRUS-W: Commissioning and First-Year Results of a New Integral Field Unit Spectrograph Dedicated to the Study of Spiral Galaxy Bulges

Maximilian H. Fabricius[a,b] and Frank Grupp[a,b] and Ralf Bender[a,b] and Niv Drory[c] and Jim Arns[d] and Stuart Barnes[e] and Claus Gössl[a] and Jan Snigula[a,b] and Gary J. Hill[c] and Ulrich Hopp[a,b] and Florian Lang-Bardl[a] and Phillip J. MacQueen[e] and Roberto Saglia[b] and Philipp Wullstein[f]

[a]University Observatory of the Ludwig-Maximilians University (LMU), Munich, Germany;
[b]Max-Planck Institute for Extraterrestrial Physics (MPE), Munich, Germany;
[c]Instituto de Astronomia, Universidad Nacional Autonoma de Mexico (UNAM), Mexico, D.F.;
[d]Kaiser Optical Systems, Inc., Ann Arbor, MI. USA;
[e]McDonald Observatory and Department of Astronomy, University of Texas at Austin, USA
[f]Max-Planck Institute for Astrophysics (MPA), Munich, Germany;

## ABSTRACT

In November and December 2010 we successfully commissioned a new optical fibre based Integral Field Unit (IFU) spectrograph at the 2.7 m Harlan J. Smith Telescope of the McDonald Observatory in Texas. Regular science observations commenced in spring 2011. The instrument achieves a spectral resolution of $\lambda/\Delta\lambda = 8700$ with a spectral coverage of 4850 Å − 5480 Å and a spectacular throughput of 37% including the telescope optics. The design is related to the VIRUS-P instrument that was developed for the HETDEX experiment, but was modified significantly in order to achieve the large spectral resolution that is needed to recover the dynamical properties of disk galaxies. In addition to the high resolution mode, VIRUS-W offers a stellar population mode with a resolution of $\lambda/\Delta\lambda = 3300$ and a spectral coverage of 4340 Å − 6040 Å. The IFU is comprised out of 267 150 $\mu m$-core optical fibers with a fill factor of 1/3. With a beam of f/3.65, the core diameter translates to 3.2″ on sky and a large field of view of 105″ × 55″ that is ideally suited to study the bulge regions of local spiral galaxies. The large throughput is due to a design that operates close to the numerical aperture of the fibers, a large 200 mm aperture refractive camera with no central obscuration, highly efficient volume phase holographic gratings, and a high-QE CCD. We will discuss the design, the performance and briefly present an example for the very up-to-date science that is possible with such instruments at 2 m class telescopes.

**Keywords:** Integral Field Unit, IFU, optical fibers, spectrograph, Wendelstein

## 1. INTRODUCTION

In May 2012 the new 2 m Fraunhofer telescope on top of the mountain Wendelstein in Bavaria, Germany[1] was officially inaugurated. The telescope was built by and is operated by the University Observatory in Munich. In parallel to its construction we are developing a number of instruments, namely the Wendelstein Wide Field Imager (WWFI[2]), the Optical-NIR Multi-Channel Imager (3kk[3]), an upgrade to the FOCES Echelle Spectrograph,[4,5] and the here discussed fiber based Integral Field Unit (IFU) Spectrograph VIRUS-W, first presented at the SPIE 2008.[6] The name VIRUS-W is owed to the heritage of the instrumental design from the VIRUS spectrograph for the HETDEX experiment.[7,8] A prototype of this instrument – the Mitchell Spectrograph (formerly VIRUS-P; VP hereafter) – is already in operation[9] and has successfully demonstrated its science capability in several published studies.[10–14]

Further author information: (Send correspondence to Maximilian H. Fabricius)
Maximilian H. Fabricius: E-mail: mxhf@mpe.mpg.de, Telephone: +49 (0)89 30000 3779

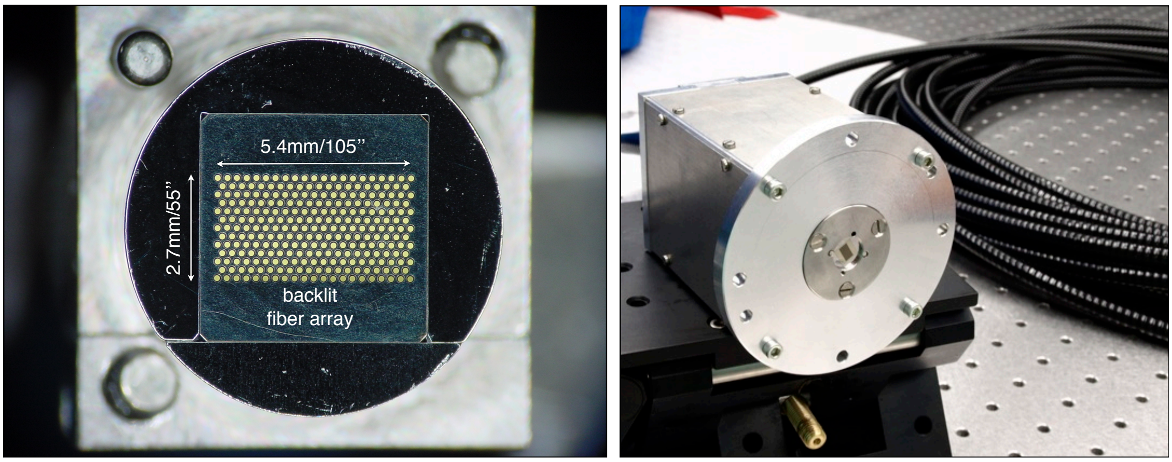


Figure 1. The Integral Field Unit (IFU) of the spectrograph. *Right panel:* The complete mechanical package that is attached to the telescope. The aluminium parts were coated black after this image was taken. The 25 m long fiber cable can be seen in the background. *Left panel:* Micrograph of the IFU. The 267 fibers are arranged in a hexagonal densepack scheme. The total fill factor is 1/3. The fiber slit was illuminated while this image was taken.

The instrument was completed in mid 2010. As the Wendelstein telescope was not completed at that point we shipped the instrument to the McDonald Observatory for a temporary stay. The similarity to the VP spectrograph assured a very smooth commissioning in November and December 2010 at the 2.7 m Harlan J. Smith Telescope. VIRUS-W has since been in normal operation and already contributed to a number of scientific programs concerned with the dynamics of galaxies.

VIRUS-W increases the spectral resolution of the VP design. A $R \simeq 8700$ mode is dedicated to kinematically cold systems like disks and pseudobulges of spiral galaxies and resolves velocity dispersions down to 15 km $s^{-1}$. An additional lower resolution mode ($R \simeq 3300$) with a broader spectral coverage gives access to a larger number of absorption features for the study of stellar population parameters such as ages and metallicities. The individual fibers have a diameter of $3.2''$ on sky at the 2.7 m and as such sacrifice spatial resolution for the benefit of high spectral resolution and a large field of view (FoV) of $150'' \times 75''$. This combination of a relatively high spectral resolution and large field coverage is a unique feature of VIRUS-W which will allow us to tackle pressing questions of modern astronomy such as the dark matter distributions in local low surface brightness systems and the formation mechanisms of different bulge types of spiral galaxies.

In the next section we will first give a brief overview on the optical design. In Section 3 we will then give account of the optical characteristics, the achieved throughput, and the instrumental resolution. In Section 4 we will give an example for the data that can be obtained with such an instrument. Finally in Section 5 we will conclude and very briefly show an example for the type of science that can be done with such an instrument at hand.

## 2. OPTICAL DESIGN

### 2.1 Integral Field Unit

The IFU is constructed from 267, 150 $\mu m$ core optical fibers (Polymicro, FVP150165195). They are arranged into a rectangular array in a hexagonal densepack scheme with a fill-factor of 1/3 (see Fig. 1). A focal reducer in front of the IFU converts the f/8.8 beam which is delivered by the 2.7 m into an f/3.65 beam which is accepted by the fibers. In the high resolution mode we place a SDSS $g$ filter in front of the focal reducer to suppress wavelengths that fall outside of the covered spectral range and would create stray light otherwise. The fibers are glued into a drilled stainless steel matrix. The package was polish after the glueing of the fibers. The manufacturing of the IFU was carried out by FiberTech in Berlin, Germany. An anti-reflective coated 1 mm think glass plate is placed directly in front of the fibers. The gap between the fiber surfaces and the glass plate is filled with an

Table 1. Characteristics of the Integral Field Unit

| | |
|---|---|
| **Physical** | |
| Fiber core size | 150 $\mu m$ |
| packing | hexagonal densepack |
| number of rows | 13 $\mu m$ |
| number of fibers within one row | 21/20, alternating |
| fill factor | 1/3 |
| physical dimension of IFU | 5.46 mm $\times$ 2.96 mm |
| **At 2.7 m and $f/\#$ 3.65** | |
| fiber core diameter | 3.14$''$ |
| IFU field of view | 105$''$ $\times$ 55$''$ |
| **At 2.0 m and $f/\#$ 3.65** | |
| fiber core diameter | 4.2$''$ |
| field of view | 144$''$ $\times$ 75$''$ |

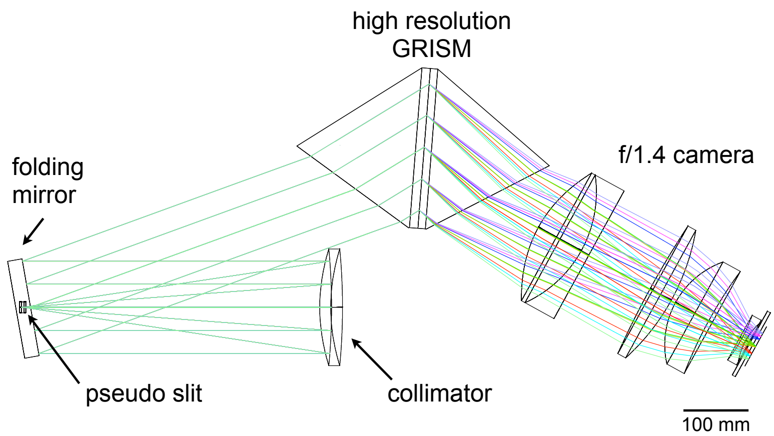


Figure 2. Layout of the spectrograph in the high resolution mode. The light enters the spectrograph on the left hand side through the pseudoslit which is located in a slot within a flat folding mirror. The slit is oriented perpendicular to the image plane in this figure. In the high resolution mode a combination of two large prisms and a 3300 ll/mm VPH grating – a GRISM – act as dispersive element. Note, the prisms add little to the dispersive power of the grating. Their primary function is to couple the light into, and out of the grating. Further, their geometry is chosen such that the camera location stays fixed between the two resolution modes. The 200 mm aperture, $f/1.4$ camera on the right-hand side records the spectra. In the low resolution mode, the GRISM is replaced by a 1900 ll/mm 160 mm $\times$ 170 mm large VPH grating which is sandwiched between two plane parallel fused silica plates.

index matching gel. This *normalizer plate* serves to heal residual imperfections from the polishing process of the fibers. A chrome oxide coating was applied to the glass plate to mask out the relatively high reflective surface that surrounds the fibers.

The complete mechanical package of the IFU is relatively small (about 80 mm $\times$ 50 mm $\times$ 50 mm) and allows for fast exchange between the VIRUS-W and the VP spectrograph. The fibers are routed in a 25 m long bundle from the telescope focal station into the control room where the spectrograph is located. Table 1 gives account on the detailed layout of the IFU.

## 2.2 Spectrograph

The spectrograph uses as an inverse Schmidt type design for the collimation of the light (see Fig.2). The light enters the instrument through 267 optical fibers which are spread out into a 76 mm long pseudo slit. A cylindrical normalizing lens which is again coupled with index matching gel against the fiber end surfaces minimizes light scattering due to polishing residuals. The fibers face a spherical collimator which reflects the light back into the direction of the fibers. Those are located within a slot of a flat folding mirror which then directs the light to the dispersive element. Both mirrors are coated with an enhanced aluminium coating with a mean reflectivity of 95% over the covered wavelength range. The fiber slit design and the mirror system are essentially identical to the VP design and we refer the reader to the corresponding publications for further details.[7,8]

We use two Volume Phase Holographic (VPH) Gratings from Kaiser Optical Systems Inc. in first order for the dispersion of the light. These gratings offer large throughput at high line densities with very low amounts of scattered light. The low resolution mode grating is sandwiched between two plane parallel fused silica plates. Two large prisms which are glued the entrance and the exit surface of the high resolution mode grating serve to decrease the internal angle of incidence at the exit surface in order to prevent total internal refraction. Also the exact choice of the prism angle allows us to keep the camera position fixed between the exchange of the gratings which simplifies the mechanical design significantly. Table 2 lists the physical parameters of the gratings. With peak values of 70% and 87% the high and low resolution gratings have impressive diffraction efficiencies and are largely responsible for the very high instrumental throughput (see Section 3).

A 200 mm large aperture fully refractive f/1.4 camera records the spectra. The optics comprised out of five lenses in four groups where the entrance and the exit surfaces are aspheres. The refractive design avoids the central obscuration of the original VP design and result in an improved throughput. The detailed surface description is given in our 2008 paper.[6] The first group can be adjusted for focus and is equipped with a stepper drive. The camera lens was manufactured by POG Precision Optics Gera GmbH in Germany.

We use a Marconi (today e2v) CCD44-82 back side illuminated CCD with 2048 × 4096 15 $\mu m$ square pixels. This detector is one of the spare OmegaCam[15] detectors and the quantum efficiency was determined by the detector lab of the European Southern Observatory (ESO). It varies between 80% and 85% with a mean value of 83% in the covered spectral range. This CCD is actually somewhat larger than the footprint of the originally proposed spectral range.[6] This high optical quality of the camera lens allowed us to extend the spectral range to 4850Å– 5475Å(4340Å– 6042Å) in the high (low) resolution mode. The company Spectral Instruments Inc. integrated this CCD into their SI 1100 camera head which provides the readout electronic and cryogenic cooling through a Polycold Cryotiger closed cycle system. The camera head is decoupled from the lens and equipped with its own vacuum window. Its is mounted at the lens exit with three fine threaded screws which allow us to adjust for tip tilt and piston. The fast camera optics make a fine adjustment capability of the detector position essential. The decoupling of the camera head from the lens however results in a relatively easy non-cryogenic procedure. The SI 1100 electronics allows for multiple readout modes. In the standard science mode the detector is read out over two amplifiers at 110 kHz with a gain of 1.61 ADU/$e^-$ and a read noise of 2.55 $e^-$[*].

The spectrograph mounted on a 1600 mm × 1200 mm optical bench and, at the McDonald Observatory, located in the control room. The constant gravity vector and the stable temperature environment results a high instrumental stability. To compensate the residual temperature swings of the control room we insulated the inside of the enclosure with Armaflex attached heating panels which are controlled by a standard PID process controller. The Wendelstein Observatory is equipped with a dedicated spectrograph room underneath the telescope dome.

# 3. INSTRUMENTAL PERFORMANCE

With the commissioning data at hand we can asses key instrumental characteristics such as instrumental throughput and spectral resolution. The data reduction and the extraction of individual fiber spectra is done through a slightly modified version of the HETDEX pipeline `cure` that we develop in Munich. This pipeline will be discussed elsewhere in detail. Following standard procedures for frame cropping, rotation, the subtraction of the bias signal, and the creation of master calibration frames, `cure` fits a two-dimensional Chebyshev polynomial of

[*] The gain and read noise were measured by Spectral Instruments Inc.

Table 2. Characteristics of the dispersive elements

| | |
|---|---|
| **High resolution mode** | |
| Grating physical dimensions | 170 mm × 220 mm × 24 mm with two prisms attached |
| Line frequency | 3300 ll/mm |
| Blaze wavelength | 5193 Å |
| Angle of incidence | 35.9 ° in fused silica. |
| Angle of diffraction | -35.9 ° in fused silica. |
| Substrate material | fused silica |
| Mean diffraction efficiency | 58 % |
| **Low resolution mode** | |
| Physical dimensions | 170 mm × 180 mm x 24 mm |
| Line frequency | 1600 ll/mm |
| Blaze wavelength | 5170 Å |
| Angle of incidence | 19.7 ° in fused silica, 24.4 ° in air. |
| Angle of diffraction | -13.3 ° in fused silica, -19.6 ° in air. |
| Substrate material | fused silica |
| Mean diffraction efficiency | 86 % |

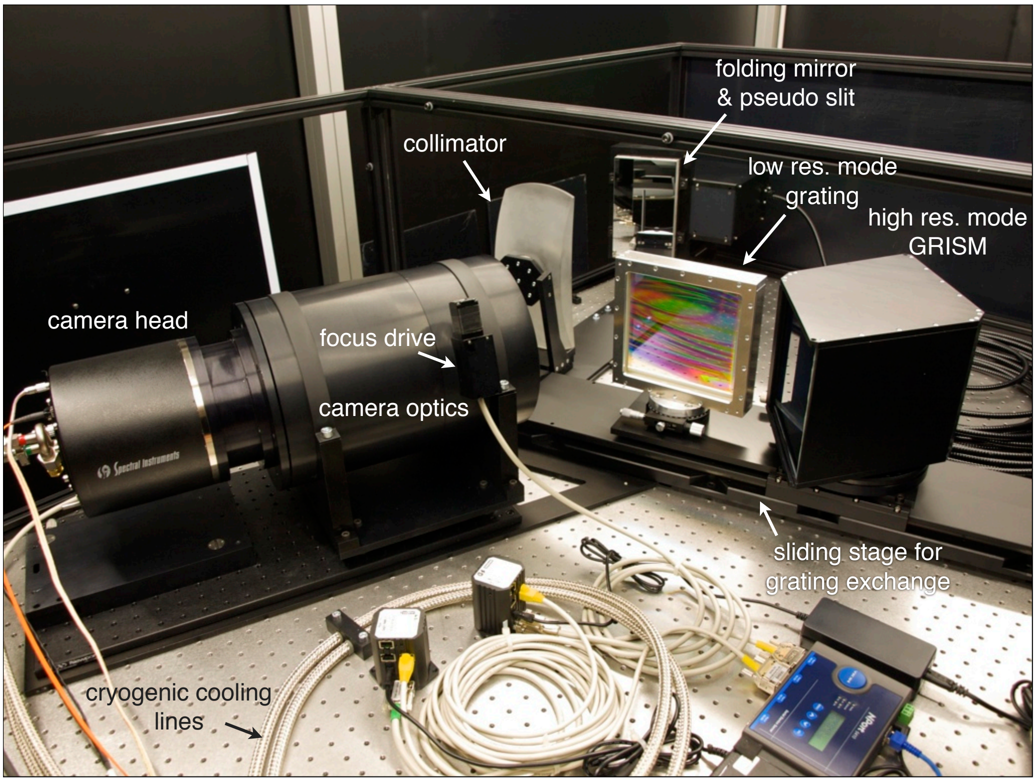


Figure 3. The complete spectrograph assembled. The image was taken in the optical laboratory in Munich shortly before the instrument was packed and shipped to the McDonald Observatory. The devices seen in the bottom half are the motor controllers for the grating exchange and the camera focus drive, the ethernet to RS232 converter, and power supplies.

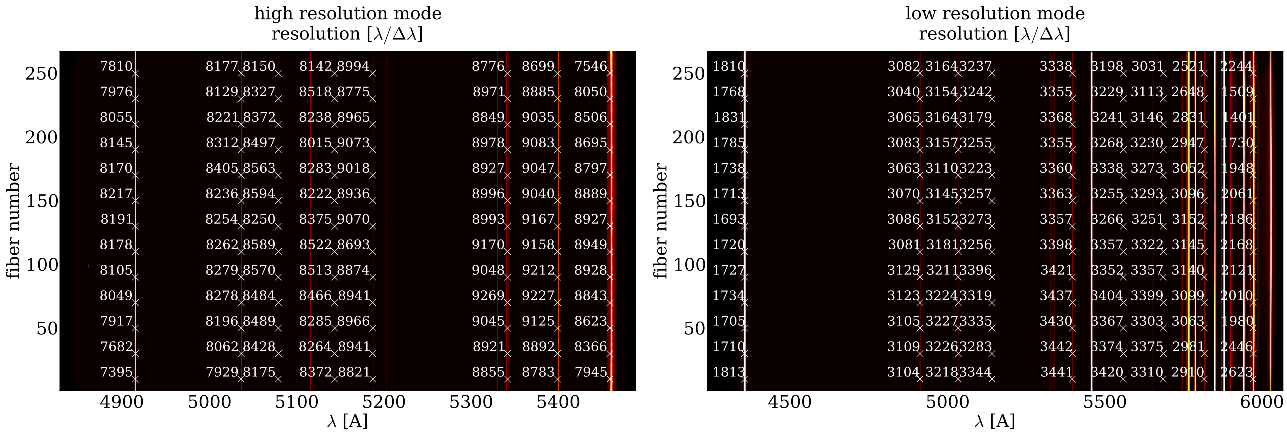


Figure 4. The resolution as calculated from the calibration lamp frames (see text). We plot the wavelength calibrated and fiber extracted spectra in the background and indicate the lines and positions that were used to calculate the resolution $R = \lambda/\Delta\lambda$. The labelled values are the median of a measurement of 20 neighbouring fibers.

| | |
|---|---|
| **High Resolution Mode** | |
| **spectral coverage** | 4850 Å– 5475 Å |
| **resolution ($\Delta\lambda/\lambda$)** | 7395 to 9270 (depending on wavelength); mean: 8660 |
| **resolution ($\sigma$)** | 14 kms$^{-1}$ to 17 kms$^{-1}$; mean: 15 kms$^{-1}$ |
| **linear dispersion** | 0.19 Å/px |
| **Low Resolution Mode** | |
| **spectral coverage** | 4340 Å - 6042 Å |
| **resolution ($\Delta\lambda/\lambda$)** | 1705 to 3400 (depending on wavelength); mean: 3275 |
| **resolution ($\sigma$)** | 28 kms$^{-1}$ to 75 kms$^{-1}$; mean: 38 kms$^{-1}$ |
| **linear dispersion** | 0.52 Å/px |

Table 3. Resolutions and spectral coverage for the two different modes of resolution.

7-th degree to the mapping of fiber number and wavelength to x and y pixel position on the detector. It also computes inverse and cross transformation which are then subsequently used for the extraction of fiber spectra.

The wavelength calibration uses a combination of Ne and Hg lamps. We typically fit 19 lines in the high resolution mode and 34 lines in the low resolution mode. The linear part of the spectral dispersion is in good agreement with the expectations from the optical design. We find values of 0.19 Å/px (0.52 Å/px) in the high (low) resolution mode in the chip center. The typical standard deviation of the wavelength calibration is 0.2 pixel or 0.04 Å in the high resolution mode and 0.1 Å in the low resolution mode.

By fitting Gaussians to the line profiles in the spectral direction we obtain the spectral resolution as $R = \lambda/\Delta\lambda$ where $\Delta\lambda$ is the FWHM of the fitted Gaussian profile. We average the line profile over 20 neighbouring fibers to increase the signal to noise. We also select for non-blended and bright calibration lines. Fig. 4 shows the resolution as a function of chip position. The spectral resolution varies as a consequence to the spatially varying instrumental point spread function. For the high resolution mode we find values from $R = 7395$ ($\sigma_{inst} = c/R \cdot 2.35 = 17.3\,\mathrm{kms}^{-1}$) to $R = 9270$ ($\sigma_{inst} = 13.8\,\mathrm{kms}^{-1}$) with a mean value of $R = 8660$ ($\sigma_{inst}$ =14.7 kms$^{-1}$). In the low resolution mode we obtain $R = 1705$ ($\sigma_{inst} = 74.8\,\mathrm{kms}^{-1}$) to $R = 3400$ ($\sigma_{inst} = 28.0\,\mathrm{kms}^{-1}$) with a mean value of $R = 3275$ ($\sigma_{inst} = 37.5\,\mathrm{kms}^{-1}$) in the low resolution mode. Table 3 summarizes the spectral resolution and coverage for the two different modes.

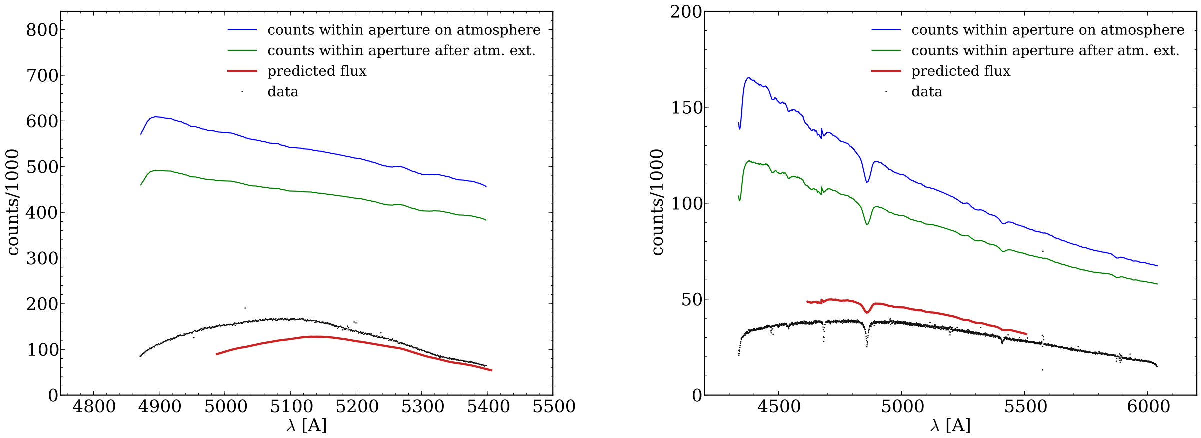


Figure 5. Comparison of the predicted flux of the spectrophotometric standard Feige 110 based on the published data[16] to the measured fluxes (see text). The predicted fluxes are corrected to the effective airmass of the observation.

We have obtained observations of the spectrophotometric standard star Feige 110. Since the fill factor of the IFU is 1/3 we obtained multiple observations offset with respect to each other such as to fill the gaps between the fibers. In principle three of these dithered observations will result in a 100% fill. We repeat this ditherset once, offset by half a fiber diameter from the original position, for increased accuracy. The summed flux of all fiber spectra can then be compared to the prediction that is based on the publish data.[16] We calculate atmospheric extinction losses using the IRAF ONEDSPEC extinction law for the Kitt Peak Observatory (altitude 2096 m, McDonald 2070 m). We model the telescope with three reflections of pure aluminium mirrors and assume newly coated mirrors. We use a 2.7 m aperture and a 43 cm wide central obscuration from the secondary mirror. We use transmission values for the fibers provided by Polymicro (mean 92%). For the focal reducer, air-glass surfaces and the camera lens surfaces we assume a 1% loss due to reflections. For the filter, the mirrors, and the gratings we use the reflectivity and efficiency values that were provided by the manufacturers. Finally we use the ESO determined value for the quantum efficiency of the detector.

We find reasonable agreement between the predicted and the measured counts (see Fig. 5). For the high resolution mode we find with a peak value of 37 % actually an about 7 % larger throughput than the value that we expect from the prediction. This may be a consequence of pessimistic assumptions for some of the optical components and also reflect the limitation of the atmospheric model that we used. On the other hand we find a smaller then predicted throughput for the low resolution mode which peaks at 40 % while we would expect 49 %. We suspect that this is a consequence of a not yet optimally adjusted grating angle during the time of the commissioning. [†].

For exposure time calculations we fit a combination of a polynomial and a linear function (for the red end tail) to the actually measured throughputs. This eliminates the noise of the measurement and artefacts around the hydrogen absorption features that result from the different spectral resolutions of the published data and our measurements. In Fig. 6 we plot the adopted throughput models. Those include the telescope and the atmosphere at airmass one. Using typical values for the McDonald dark-time sky brightness of $22.0\,mag/''^2$ (AB) and a target surface brightness of $21.7\,mag/''^2$ (AB) we estimate to reach a signal to noise of 30 per spectral pixel within 8 hours of integration and 16 readouts of the detector (to allow for sky nods) in the high resolution mode. In the low resolution mode a signal to noise of 30 will be reached within 2 hours of integration.

[†]During a regular science run in October and November 2011 we were able to confirm incorrect grating angle setting by taking dome flats at various grating angles. Unfortunately the transparency still suffered from the severe forest fires in West Texas in the spring of the same year, leaving us unable to remeasure the actual throughput on a star.

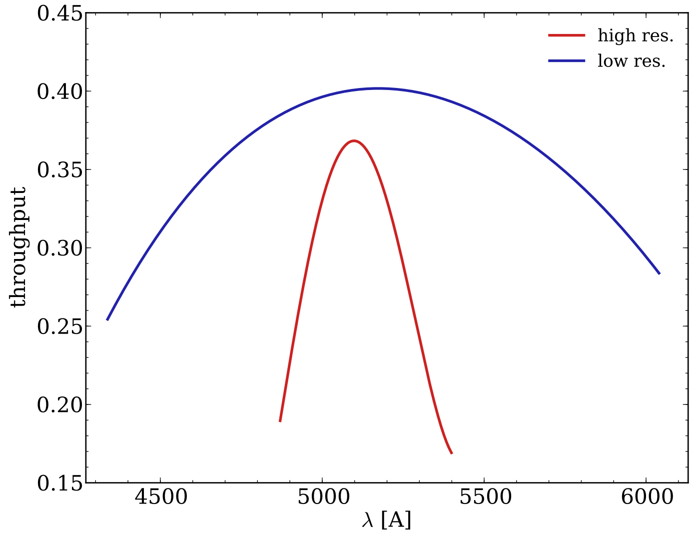


Figure 6. Smoothed throughput model for both resolution modes for airmass one. The throughput includes atmospheric loss, telescope, all optical elements between the telescope and the CCD detector, and the detector's quantum efficiency. Since VIRUS-W will observe mostly extended sources we do not include any aperture effects.

## 4. FIRST KINEMATIC MAPS

In addition to spectrophotometric standards we did observe a handful of galaxies during the commissioning runs. As an example we show the kinematic maps that we obtained for the dwarf elliptical galaxy NGC 205 in Fig. 7. This satellite of the Andromeda galaxy has a very low central stellar velocity dispersion of just $35\,\mathrm{km\,s^{-1}}$. As the stellar velocity dispersion map shows (panel d), we are able to recover these values well but also see that the dispersion drops even further down to values of about $25\,\mathrm{km\,s^{-1}}$ in the nucleus. This has been shown before in longslit data[17] that we reproduce well. The drop is certainly connected to the existence of a well known blue and young stellar component in the nucleus of this galaxy.[18,19] The velocity field (panel c) shows rotation along the major axis of the galaxy. The amplitude of the rotation across the field of view is only $5\,\mathrm{kms^{-1}}$, but this is clearly resolved by VIRUS-W.

We aim model these galaxies using the Schwarzschild method[20] to obtain the firmest constraint on the dark halo masses and central densities yet. Also, we expect to derive a more stringent constraint for the upper limit of the black hole mass in these objects than available so far.

## 5. CONCLUSION & OUTLOOK

With peak values for the throughput of 37 % and 40 % in the high and low resolution modes respectively, a FOV of and the ability to resolve velocity dispersion down to $15\,\mathrm{km\,s^{-1}}$ VIRUS-W is uniquely positioned to study the stellar kinematics of local low velocity dispersion objects. In the last section we gave a brief example for the quality of data that can be obtained with VIRUS-W. Since its commissioning in late 2010 the McDonald Time Allocation Committee granted close to 100 nights to observations which already resulted in a submitted publication[21] and several others in preparation. VIRUS-W proves that the VIRUS design can be adjusted to develop new and original instruments that have the potential to create significant scientific impact even at small to intermediate size telescopes.

With the completion of the Wendelstein telescope we will bring VIRUS-W back to Germany once the proper interfaces are in place, most likely during the second half of 2012. We are looking forward to continue several surveys that we have started which address the dynamical structure of Spiral Galaxy Bulges in dwarf galaxies.

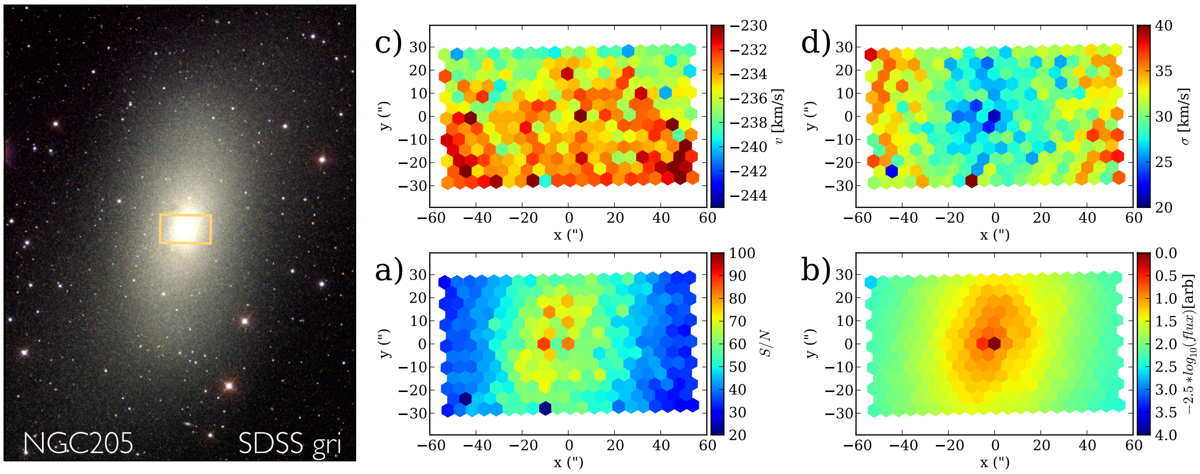


Figure 7. *Left panel:* SDSS *gri* composite and VIRUS-W FoV for NGC 205. Kinematic maps for NGC 205. Positive $y$ point to north. Negative $x$ to east. *Panel a:* $S/N$ per Å as computed by FCQ. *Panel b:* Reconstructed image with arbitrary zeropoint. *Panel c:* Mean velocity. *Panel d:* Velocity dispersion.

## ACKNOWLEDGMENTS

We wish to thank the many manufacturers who provided high quality optics and electronics. We specifically wish to point out the manufacturer of the camera cryostat Spectral Instruments and especially the help and support by Kevin Toerne. Further, we further wish to thank Präzisions Optik Gera (POG) for the production of the camera lens which in its optical quality exceeded all our expectations. We especially want to thank their executive director Aleksander Wlodarski, who personally lead the efforts of the construction of the lens. We also want to thank Manfred Groth who led the production of the large optical prisms at POG. Their optical quality is outstanding. We are greatly sorry that Manfred Groth did not live to see the completion and the success of VIRUS-W.

We would also like to express our gratitude for the help and support by the McDonald Observatory and its Staff. David Doss, Earl Green, Brian Roman, Terry Wilemon, Kevin Meyer, Darrin Crook have been extremely helpful both in preparations but also on site. We thank the McDonald TAC and directorate for allowing us to bring VIRUS-W and their willingness to accept the inconvenience that comes with such endeavours.

## REFERENCES

[1] Hopp, U., Goessl, C. A., Grupp, F., Lang, F., Mitsch, W., Relke, H., Ries, C., Wilke, S., and Bender, R., "Upgrading the Wendelstein Observatory to a 2m-class telescope," in [*Observatory Operations: Strategies, Processes, and Systems Conference - Proceedings of SPIE Volume 7016 Paper 7016-65 (2008)*], *Presented at the Society of Photo-Optical Instrumentation Engineers (SPIE) Conference* (2008).

[2] Gössl, C. A., Bender, R., Hopp, U., Kosyra, R., and Lang-Bardl, F., "Commissioning of the WWFI for the Wendelstein Fraunhofer Telescope," in [*Society of Photo-Optical Instrumentation Engineers (SPIE) Conference Series*], *Society of Photo-Optical Instrumentation Engineers (SPIE) Conference Series* (July 2012).

[3] Lang-Bardl, F., Hodapp, K., Jacobson, S., Bender, R., Gössl, C., Fabricius, M., Grupp, F., Hopp, U., and Mitsch, W., "3kk: the Optical-NIR Multi-Channel Nasmyth Imager for the Wendelstein Fraunhofer Telescope," in [*Society of Photo-Optical Instrumentation Engineers (SPIE) Conference Series*], *Society of Photo-Optical Instrumentation Engineers (SPIE) Conference Series* **7735** (July 2010).

[4] Grupp, F., Udem, T., Holzwarth, R., Lang-Bardl, F., Hopp, U., Hu, S.-M., Brucalassi, A., Liang, W., and Bender, R., "Pressure and temperature stabilization of an existing Echelle spectrograph," in [*Society of Photo-Optical Instrumentation Engineers (SPIE) Conference Series*], *Society of Photo-Optical Instrumentation Engineers (SPIE) Conference Series* **7735** (July 2010).

[5] Grupp, F., Brucalassi, A., Lang, F., Hu, S. M., Holzwarth, R., Udem, T., Hopp, U., and Bender, R., "Pressure and temperature stabilization of an existing chelle spectrograph II," in [*Society of Photo-Optical Instrumentation Engineers (SPIE) Conference Series*], *Society of Photo-Optical Instrumentation Engineers (SPIE) Conference Series* **8151** (Sept. 2011).

[6] Fabricius, M. H., Barnes, S., Bender, R., Drory, N., Grupp, F., Hill, G. J., Hopp, U., and MacQueen, P. J., "VIRUS-W: an integral field unit spectrograph dedicated to the study of spiral galaxy bulges," in [*Society of Photo-Optical Instrumentation Engineers (SPIE) Conference Series*], *Society of Photo-Optical Instrumentation Engineers (SPIE) Conference Series* **7014** (Aug. 2008).

[7] Hill, G. J., MacQueen, P. J., Tufts, J. R., Kelz, A., Roth, M. M., Altmann, W., Segura, P., Gebhardt, K., and Palunas, P., "VIRUS: a massively replicated integral-field spectrograph for HET," in [*Ground-based and Airborne Instrumentation for Astronomy. Edited by McLean, Ian S.; Iye, Masanori. Proceedings of the SPIE, Volume 6269, pp. 62692J (2006).*], *Presented at the Society of Photo-Optical Instrumentation Engineers (SPIE) Conference* **6269** (July 2006).

[8] Hill, G. J., Lee, H., Vattiat, B. L., Adams, J. J., Marshall, J. L., Drory, N., Depoy, D. L., Blanc, G., Bender, R., Booth, J. A., Chonis, T., Cornell, M. E., Gebhardt, K., Good, J., Grupp, F., Haynes, R., Kelz, A., MacQueen, P. J., Mollison, N., Murphy, J. D., Rafal, M. D., Rambold, W. N., Roth, M. M., Savage, R., and Smith, M. P., "VIRUS: a massively replicated 33k fiber integral field spectrograph for the upgraded Hobby-Eberly Telescope," in [*Society of Photo-Optical Instrumentation Engineers (SPIE) Conference Series*], *Society of Photo-Optical Instrumentation Engineers (SPIE) Conference Series* **7735** (July 2010).

[9] Hill, G. J., MacQueen, P. J., Smith, M. P., Tufts, J. R., Roth, M. M., Kelz, A., Adams, J. J., Drory, N., Grupp, F., Barnes, S. I., Blanc, G. A., Murphy, J. D., Altmann, W., Wesley, G. L., Segura, P. R., Good, J. M., Booth, J. A., Bauer, S.-M., Popow, E., Goertz, J. A., Edmonston, R. D., and Wilkinson, C. P., "Design, construction, and performance of VIRUS-P: the prototype of a highly replicated integral-field spectrograph for HET," in [*Society of Photo-Optical Instrumentation Engineers (SPIE) Conference Series*], *Society of Photo-Optical Instrumentation Engineers (SPIE) Conference Series* **7014** (Aug. 2008).

[10] Blanc, G. A., Heiderman, A., Gebhardt, K., Evans, II, N. J., and Adams, J., "The Spatially Resolved Star Formation Law From Integral Field Spectroscopy: VIRUS-P Observations of NGC 5194," *ApJ* **704**, 842–862 (Oct. 2009).

[11] Blanc, G. A., Adams, J. J., Gebhardt, K., Hill, G. J., Drory, N., Hao, L., Bender, R., Ciardullo, R., Finkelstein, S. L., Fry, A. B., Gawiser, E., Gronwall, C., Hopp, U., Jeong, D., Kelzenberg, R., Komatsu, E., MacQueen, P., Murphy, J. D., Roth, M. M., Schneider, D. P., and Tufts, J., "The HETDEX Pilot Survey. II. The Evolution of the Ly$\alpha$ Escape Fraction from the Ultraviolet Slope and Luminosity Function of $1.9 < z < 3.8$ LAEs," *ApJ* **736**, 31 (July 2011).

[12] Yoachim, P., Roškar, R., and Debattista, V. P., "Integral Field Unit Spectroscopy of the Stellar Disk Truncation Region of NGC 6155," *ApJL* **716**, L4–L8 (June 2010).

[13] Adams, J. J., Blanc, G. A., Hill, G. J., Gebhardt, K., Drory, N., Hao, L., Bender, R., Byun, J., Ciardullo, R., Cornell, M. E., Finkelstein, S. L., Fry, A., Gawiser, E., Gronwall, C., Hopp, U., Jeong, D., Kelz, A., Kelzenberg, R., Komatsu, E., MacQueen, P. J., Murphy, J., Odoms, P. S., Roth, M., Schneider, D. P., Tufts, J. R., and Wilkinson, C. P., "The HETDEX Pilot Survey. I. Survey Design, Performance, and Catalog of Emission-line Galaxies," *ApJS* **192**, 5–+ (Jan. 2011).

[14] Murphy, J. D., Gebhardt, K., and Adams, J. J., "Galaxy Kinematics with VIRUS-P: The Dark Matter Halo of M87," *ApJ* **729**, 129–+ (Mar. 2011).

[15] Deul, E., Kuijken, K., and Valentijn, E. A., "OmegaCAM: the 16k $\times$ 16k Survey Camera for the VLT Survey Telescope," in [*Society of Photo-Optical Instrumentation Engineers (SPIE) Conference Series*], J. A. Tyson & S. Wolff, ed., *Presented at the Society of Photo-Optical Instrumentation Engineers (SPIE) Conference* **4836**, 189–198 (Dec. 2002).

[16] Oke, J. B., "Faint spectrophotometric standard stars," *AJ* **99**, 1621–1631 (May 1990).

[17] Bender, R., Paquet, A., and Nieto, J.-L., "Internal stellar kinematics of three dwarf ellipticals in the Local Group," *A&A* **246**, 349–353 (June 1991).

[18] Baade, W., "The Resolution of Messier 32, NGC 205, and the Central Region of the Andromeda Nebula.," *ApJ* **100**, 137–+ (Sept. 1944).

[19] Peletier, R. F., "The Stellar Content of Elliptical Galaxies - Optical and Infrared Colour Profiles of M32 and NGC205," *A&A* **271**, 51–+ (Apr. 1993).

[20] Thomas, J., Jesseit, R., Saglia, R. P., Bender, R., Burkert, A., Corsini, E. M., Gebhardt, K., Magorrian, J., Naab, T., Thomas, D., and Wegner, G., "The flattening and the orbital structure of early-type galaxies and collisionless N-body binary disc mergers," *MNRAS* **393**, 641–652 (Feb. 2009).

[21] Jardel, R. J., Gebhardt, K., Fabricius, M. H., Drory, N., and Williams, M. *submitted* (2012).